

HYBRID THERMAL MODELLING OF COMPACTED GRAPHITE IRON DEEP-HOLE DRILLING WITH MINIMUM QUANTITY LUBRICATION

Bařış EKİM*, MUSTAFA BAKKAL*

* Department of Materials Engineering, Istanbul Technical University Graduate School of Science, Engineering, and Technology,
34469 Maslak, İstanbul, baris.ekim@uwc-usa.org

ABSTRACT

As high temperatures directly affect the physical properties of the machined surface in drilling, projecting temperatures throughout the process proved to be vital to reduce costs. Although several studies attempted to model the thermal conditions of drilling processes, only a limited number focused on the temperature distribution of the work piece. We present a novel hybrid analytical and numerical heat transfer method, through which we are able to determine the temperature distribution of a CGI work piece in MQL condition. We first describe a mechanistic approach to compute thrust and torque values, as well as heat fluxes on the chisel edge and the cutting lip using a quasi-regressive iteration approach, and heat load at the margin and the cooling effect of MQL using the inverse heat transfer method. We experimentally validate the projected temperature values, and obtain temperature distribution values for work pieces under different parameters. By comparing the theoretical and experimental data, we show that our thermal model performs well and is statistically accurate under various conditions and is a more realistic interpretation of heat generation during drilling of CGI in MQL condition.

1. INTRODUCTION

Drilling is the most common traditional machining process with the biggest part in machining time, % 41 [1]. Increased tool life, material removal rates and decreased lubrication use in drilling can provide considerable cost reduction. In the interest of reducing drilling costs, companies desire to achieve high cutting speed with less lubricant use. However, residual stress, dimensional error and the hardness of the machined surface are directly affected by high temperatures. Therefore, estimating temperatures on the final product is vital.

Nowadays, advanced cooling techniques such as MQL, CO₂ assisted MQL, and cryogenic cooling have become popular mainly in grinding and deep-hole drilling for hard-to-machine metals [2]. MQL is the most popular among these technologies, using minute amount of metal working fluid compared to other cooling technologies. Automotive powertrain

production has been especially revolutionized by this technology in the last decade [2].

Nevertheless, the cooling capacity of MQL is limited compared to flood and cryogenic cooling techniques. In this study, cooling capacity of MQL is quantified by the inverse heat transfer method.

Automotive industry aims to produce smaller, higher, and more efficient performance diesel engines that provide the legal pressure of reduced emission levels to meet customer expectations [3]. Due to the development of diesel engines, CGI usage has increased in the last two decades. As the engines operated at 135 bar in 1997, the target value of the peak firing pressure of the next generation diesel engines is expected to be 220 bar [4]. Considering the dramatic increase, a weight reduction of %10-30 can be achieved using CGI instead of grey cast iron, given the power and size of the engines [4]. CGI fulfills these requirements by providing reduced wall thickness, increased operating loads and reduced hot cracking (during shakeout) compared to grey iron, and also improved castability, heat transfer and machinability compared to ductile iron [4]. CGI is capable of being 75% stronger than grey iron due to the shape, size, and growth mechanism of graphite particles in the microstructure, which provide advanced thermal and mechanical properties [5]. To obtain and control these properties, additional alloy elements like magnesium, titanium and chromium are added to the structure; yet, these elements decrease the CGI machinability [6-8].

Several researchers have performed thermal modelling of the drilling process. Although most of these studies concentrated on drill temperatures, the number of studies focused on the prediction of work piece temperature distribution is limited. Watanebe et al. developed a finite difference model that predicts work piece temperatures to estimate thermal distortions in drilling [9]. Bono and Ni used thrust force and torque values as input in an oblique cutting to predict heat fluxes. Then, they developed an advection heat partition model to calculate the temperature distribution of the work piece in a finite element model in dry

drilling [10]. Kalidas et al. estimated heat fluxes in three distinct regions of the drill (drill body, cutting lips and chisel edge) by inverse heat conduction in dry and wet conditions [11]. Tai et al. calculated the heat flux both on the wall and on the bottom surface of the hole in dry and MQL conditions while using the inverse heat transfer method [12]. Biermann et al. also simulated the temperature work piece distribution in MQL condition by the finite element method [13, 14]. Segurajauregui and Arrazola used the inverse heat transfer model to calculate heat input to the work piece and thermal distortions [15]. Most models assumed that the heat load on the cutting edge and chisel edge is constant.

In this study, the variation of heat flux on the cutting edge is taken into account, and heat fluxes on the chisel and the cutting lip are calculated analytically. Heat fluxes at the margin, accumulated hot chips on the spiral drill flute, and the heat convection coefficient of the air-oil mixture are calculated using the inverse heat transfer method. Inverse heat transfer method has three main steps: Collecting experimental data, direct problem, and inverse problem. Experimental data is collected by embedded thermocouples 1.5 mm near the hole on the surface. Then, the direct problem is solved via a commercial finite element program named Abaqus, and the inverse problem is solved using MATLAB. The goal of this paper is to determine the temperature distribution of a CGI work piece in MQL condition using a hybrid analytical and numerical heat transfer method.

2. HEAT TRANSFER IN MQL DEEP-HOLE DRILLING

Almost all mechanical energy is converted to heat, which is shared with the tool, chip and work piece during machining. This energy is transferred to the work piece from four regions during deep-hole drilling: Chisel edge, cutting lip, drill margin, and drill flute, as illustrated in Fig. 1. The heat sources are cutting and friction on the chisel edge and the cutting lip, the friction on the drill margin, and accumulated hot chips on the drill flute.

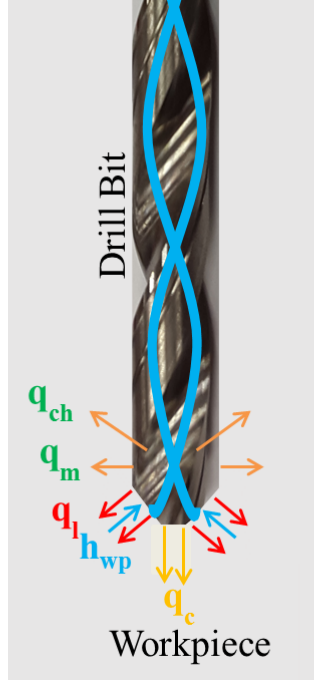


Figure 1. The heat sources during deep-hole drilling

Two major heat sources are precipitated from cutting on the cutting lip (q_l) and the chisel edge (q_c). Figure 2 shows where heat generates in the cutting process. A large amount of heat is generated in the shearing zone (zone a in Fig. 2) because of high thermo-mechanical deformation. In addition, the friction between the chip and tool rake face (zone b in Fig. 2), as well as the friction between the machined surface and tool flank surface (zone c in Fig. 2) are the other regions of generated heat. The friction between the tool margin and hole walls (q_m) and accumulated hot chips (q_{ch}) through the flute are minor heat sources. Besides, lubrication fluid (h) is widely used to cool the drill and work piece, and evacuate the hot chips. In this study, MQL was used to cool the work piece by convection during deep-hole drilling. The cooling effect of MQL on the bottom and on the hole surface is taken into account in the temperature distribution calculation. Heat generation loads at the cutting lip and at the chisel edge were calculated analytically. The convection coefficient of the air-oil mixture and the combination of heat generation at the margins and accumulated hot chips on the flutes were calculated by the inverse heat transfer method.

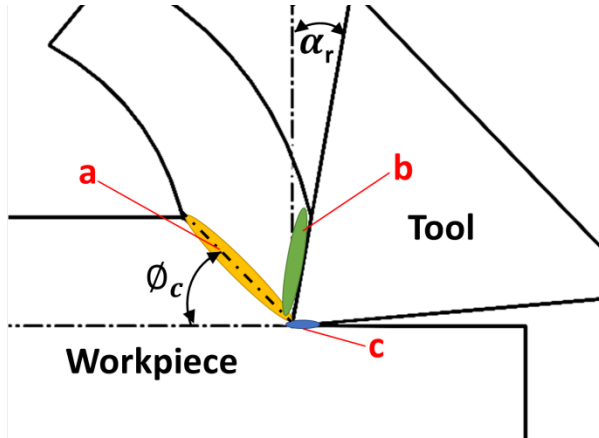


Figure 2. Heat generation regions

3. HEAT FLUX CALCULATIONS

The heat flux calculation procedure includes the geometric model of the drill, the prediction of the cutting force and the torque values at the cutting lip and the chisel edge. While estimating the cutting force, the cutting lip and chisel edge were divided to segments because of varying inclination and rake angles, namely the Elemental Cutting Tools (ECTs). The advection heat partition model developed by Bono and Ni [10] was applied to obtain the heat flux on cutting surface for each ECT. The total amount of heat generated by each ECT by shear and friction in the first and second regions can be calculated using

$$q = q_{shear} + q_{friction} = T \cdot \omega + F_z \cdot V_f \quad (1)$$

The heat partition ratio, or the ratio of total heat transfer to the work piece, can be determined using

$$r = \frac{F_u V_{chip}}{T_w + F_z V_f} \quad (2)$$

where V_{chip} is the chip velocity and F_u is the friction force between the rake face and the chip.

These expressions can be derived using the following equations:

$$V_{chip} = V \frac{\cos(i) \sin(\phi)}{\cos(\eta) \cos(\phi - \alpha)} \quad (3)$$

$$F_u = \frac{(\cos(\alpha)\cos(\eta))F_t + (\sin(\alpha)F_f)}{\cos^2(\alpha)\cos(i)\cos(\eta) + \sin(\alpha)(\sin(i)\sin(\eta) + \sin(\alpha)\cos(i)\cos(\eta))} \quad (4)$$

Total heat generation rates at the cutting lip and the chisel edge per area on the work piece can be calculated using

$$q_{wp}'' = \frac{(1-r)(Tw+F_zV_f)}{\pi(r_{out}^2 - r_{in}^2)} \quad (5)$$

Cutting force analyses were conducted in the two regions: The chisel edge and the cutting lip, in the previous study [16]. Generated thrust force and torque at the chisel edge are studied by dividing the chisel edge into two parts in this study as well. An indentation mechanism is used at the center of the chisel and orthogonal cutting mechanics are used in the cutting region between the center of the drill and chisel edge-lip intersection. Thrust force and torque at the cutting lips were examined by using oblique cutting mechanics by means of discretizing the cutting edges to the small sections.

The heating effect of the drill margin and the accumulated hot chips, and the cooling effect of the oil-air mixture on the hole wall were taken into account simultaneously. The inverse heat transfer method was used to calculate heat flux on the hole wall. Heat flux at the margin was assumed to be exponential and constant after 1mm. Also, the cooling effect of MQL on the hole wall was implemented to the exponential heat flux equation as

$$q_m = q_{ma} \cdot e^{-q_{mb}} \quad (6)$$

where q_{ma} and q_{mb} are coefficients. In addition, the cooling effect of the pressurized oil-air mixture on the chisel edge and the cutting lip are defined as the convection coefficient h . This coefficient was also assumed to be time-independent throughout the drilling process and applied uniformly.

In the inverse heat transfer method, the procedure consists of three different parts: Experimental data collection, direct solution and inverse solution. Direct solution was described in the finite element simulation section, and the inverse solution was computed by the optimization toolbox in MATLAB. The aim of the inverse solution is to compute the air-

oil mixture convection coefficient and the heat flux at the margin and the flute by minimizing the objective function. The objective function is the absolute value of the differences between the calculated and measured temperatures. It can be represented as

$$f_{objective} = \int_{t_0}^{t_f} (|T_{measured} - T_{calculated}|) dt \quad (7)$$

The optimization scheme of the inverse heat transfer problem is given in Figure 3. The direct problem is solved by Abaqus in all iterations, while the numerical and experimental results are compared and the revised heat flux value is predicted by MATLAB. MATLAB has the function fmincon in its optimization toolbox, using which the objective function was minimized in order to estimate the heat convection coefficient of the air-oil mixture and the heat flux at the margin.

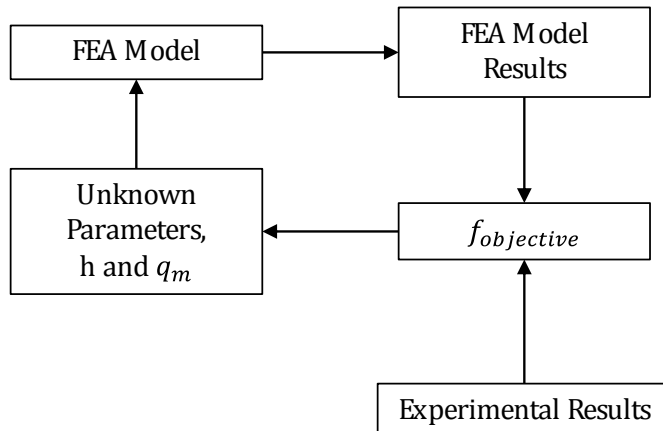


Figure 3. The optimization scheme of the inverse heat transfer problem.

4. FINITE ELEMENT MODEL

Abaqus Standard Commercial Software was used to solve 2D transient heat transfer problems. In this model, 10563 four node linear axis-symmetric quadratic elements (DCAX4) were used. Temperature-dependent material properties were taken into account and described in the experimental setup section. The heat convection coefficient of air was set to $20 \text{ W/m}^2\text{K}$ and applied to free surfaces except hole surfaces. 251 calculation steps were defined and each calculation step time was determined depending on the cutting parameters.

Fig. 4 illustrates the concept of the FEA model. The chisel edge and the cutting lip were divided by two and five elements, respectively. At step i , the heat fluxes calculated with respect to the distance of the ECT position to the center of drill were applied to elements. Heat fluxes on the hole wall due to friction and hot chips were calculated by the inverse heat transfer method and it was assumed to be exponential and kept constant after 1 mm. The convection coefficient of the air-oil mix was also applied to the bottom surface of the hole. The temperature distribution was then solved with respect to these boundaries and loaded conditions presented in Fig. 4. At step $i+1$, a layer of elements applied to the heat flux on the hole bottom was removed and the temperature distribution results at step i were used as initial conditions. The same boundaries and conditions were applied to following elements to solve temperature distributions at step $i+1$. The cycle was repeated throughout the entire drilling process. This loop expresses the moving heat source and chip removal process.

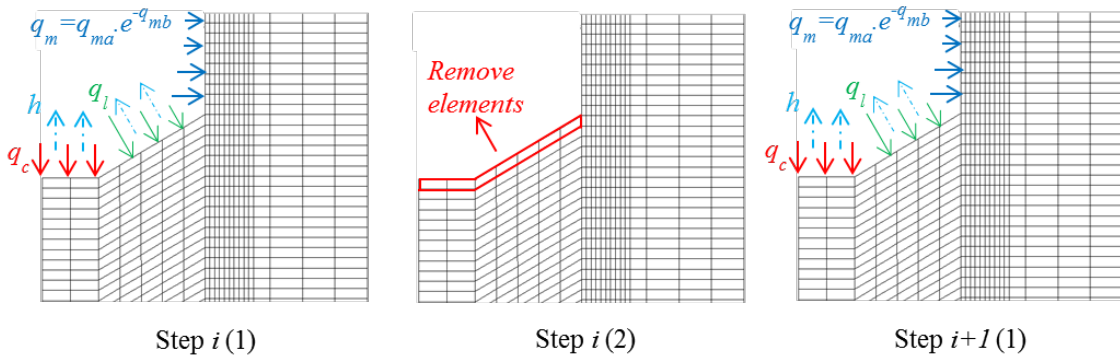


Figure 4. The concept of FEM solution

5. EXPERIMENTAL SET-UP

Drilling experiments were conducted on a YCM GT200A CNC turning machine. In this system, the drill was stationary and the MQL was connected directly to the drill shank. It is to be noted that during all of these operations, the cutting temperature was measured by using embedded thermocouples in several points simultaneously. The schematic of the deep-hole drilling setup and the thermocouple locations are illustrated in Figure 5, where A

indicates the data logger and B indicates the balanced weight and bridge slice together. Bridge slices were used to connect thermocouples to the data logger. The DTS slice nano data logger with three dimensions was used to collect temperature data on the rotating work piece. The data logger fixed to the chuck can collect the data using its battery and internal memory at a rate of 12000 Hz. This data recorder captures the drilling operation temperature by using two K-type embedded thermocouples located at a distance of 1.5 mm from the drilled surface. These thermocouples were attached 25 and 75 mm away from the top surface. Two weights were mounted on the chuck in order to maintain balance and avoid additional vibration.

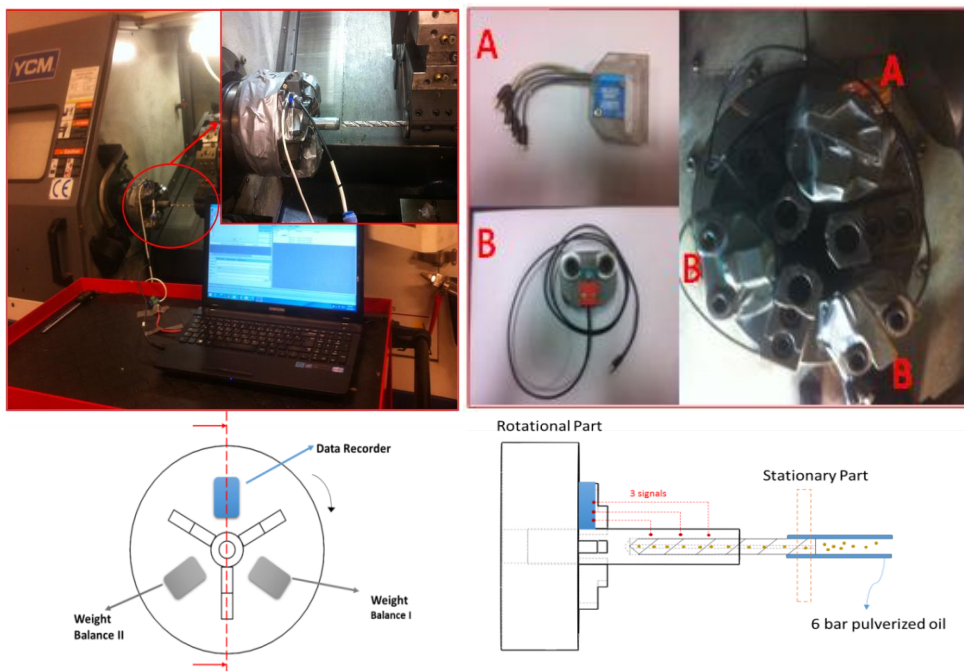


Figure 5. MQL assisted deep-hole drilling temperature measurement setup

The work piece material CGI is 20 mm in diameter and 200 mm in length. The grade of CGI is GJV 400 with $7,150 \text{ kg/m}^3$ density, 39 W/m-K thermal conductivity, and 475 J/kg-K specific heat ratios. A two-flute uncoated solid carbide, a 10 mm diameter drill with a 30° helix angle, 118° point angle, 120° chisel angle, a pitch length of 50 mm, chisel length of 2.55 mm and core diameter of 3 mm, were used. The cutting tests were conducted using three different cutting parameter sets, given in Table 1.

Table 1. Parameters for the deep-hole drilling experiment.

MQL properties		
Air	6 bar	
Oil flow rate	100 ml/hr	
Viscosity of oil (@ 40°)	47 mm ² /s	
Density (@ 20°)	0.92 g/ccm	
Ignition temperature	265°	
Tool properties		
Helix angle	30°	
Cone angle	118°	
Pitch length	50 mm	
Drill diameter	10 mm	
Chisel angle	120°	
Chisel length	2.55 mm	
Core diameter	3 mm	
Cutting parameters		
Exp #	Cutting speed [m/min]	Feed [mm/rev]
I	25	0.15
II	50	0.15
III	75	0.1

6. RESULTS

6.1. Distribution of heat flux on the cutting edge

The conducted heat into the work piece was calculated as a heat flux on the chisel and the cutting lip for each ECT using Eq. 6. The heat fluxes into the work piece are depicted in Figure 6. For all cutting parameters, the heat generation rate decreases on the cutting edge, even though the torque is higher due to the area of the elements increasing with the radius. A linear relationship was observed between cutting speed and heat generated. Heat generated by Exp. II towards the cutting edge with 50 m/min cutting speed was almost twice that of Exp. I with 25 m/min (half of Exp. I) cutting speed in same feed value. Although the cutting speed increased from (Exp. II) 50 m/min. to (Exp. III) 75 m/min, difference in heat generated was not significant. It can be presumed from this analysis that the energy needed to drill CGI decreases while the higher feed value results in higher torque.

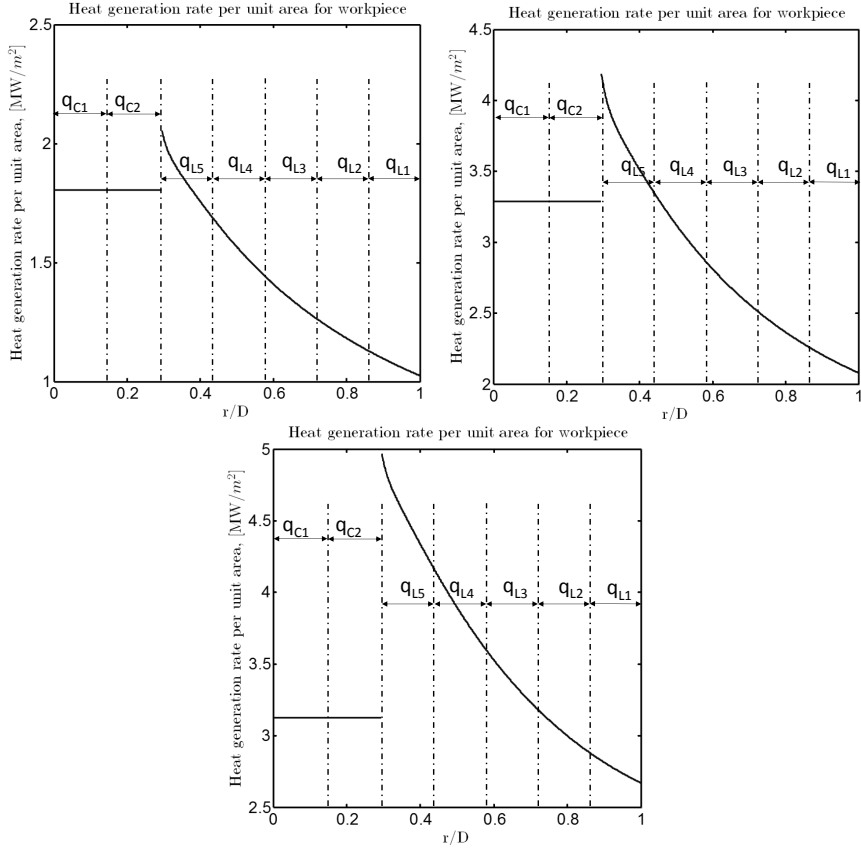


Figure 6. The conducted heat into the work piece. a) $V_c=25 \text{ m/min}$ $f=0.15 \text{ mm/rev}$ b)
 $V_c=50 \text{ m/min}$ $f=0.15 \text{ mm/rev}$ c) $V_c=75 \text{ m/min}$ $f=0.1 \text{ mm/rev}$

6.2. The heat generation rates at the margin and convection coefficients

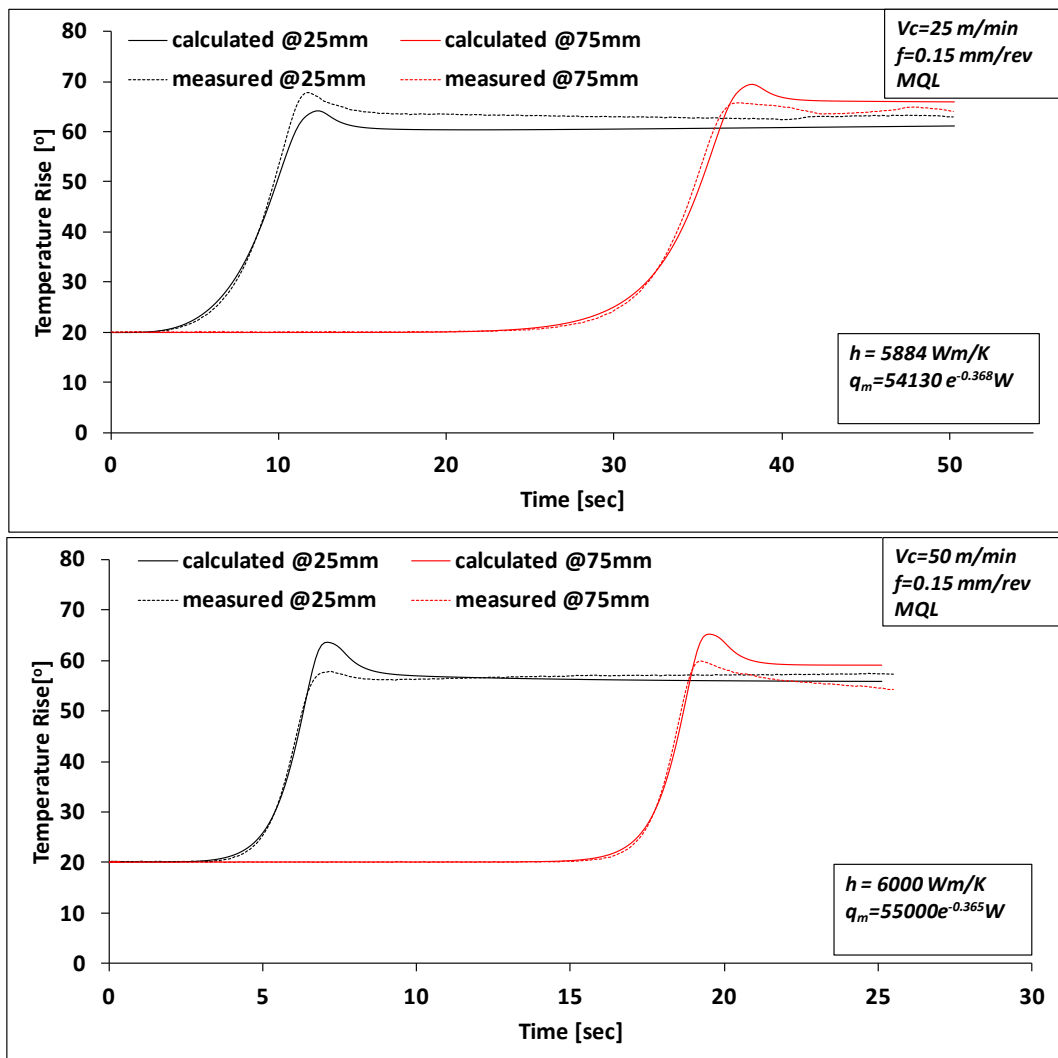
The heat generation rates at the margin and the convection coefficient of the air-oil mixture were estimated using an inverse heat transfer method. The heat generation rate at the margin also includes the cooling effect of MQL and the accumulated hot chips. Calculated heat flux coefficients at the drill margin and the convection coefficient of air-oil mixture are given in Table 2 for each experiment. q_m , defined in Eq. 6, indicates the maximum value of the margin heat fluxes. It decreases exponentially with distance from the drill tip, and it is kept constant after 1 mm at $q_m/8$. The convection coefficient of the air-oil mixture was calculated similarly in Exps. I and II, which were carried out using the same feed. The heat convection in Exp. III was estimated to be lower than that of Exp I and II, which shows that the cooling capacity can change according to cutting speed and feed. However, it is difficult to distinguish which factor is more prominent than the others.

Table 2. Calculated heat flux coefficients at the drill margin and convection coefficient

Exp.	Cutting Speed [m/min]	Feed [mm/rev]	q_{wa}	q_{wb}	h [W/m ² K]
I	25	0.15	21558	-0.416	5844
II	50	0.15	55000	-0.365	6000
III	75	0.1	43740	-0.398	4498

6.3. Validation of temperatures

The calculated temperatures via the advection FEA model were validated by comparing the experimentally measured temperatures at two points. Calculated and measured temperatures during the deep-hole drilling process are given in Fig. 7. Favorable agreements were obtained between experimental and predicted temperature distribution results, and it can be seen that the model represents the heating and cooling rates accurately.



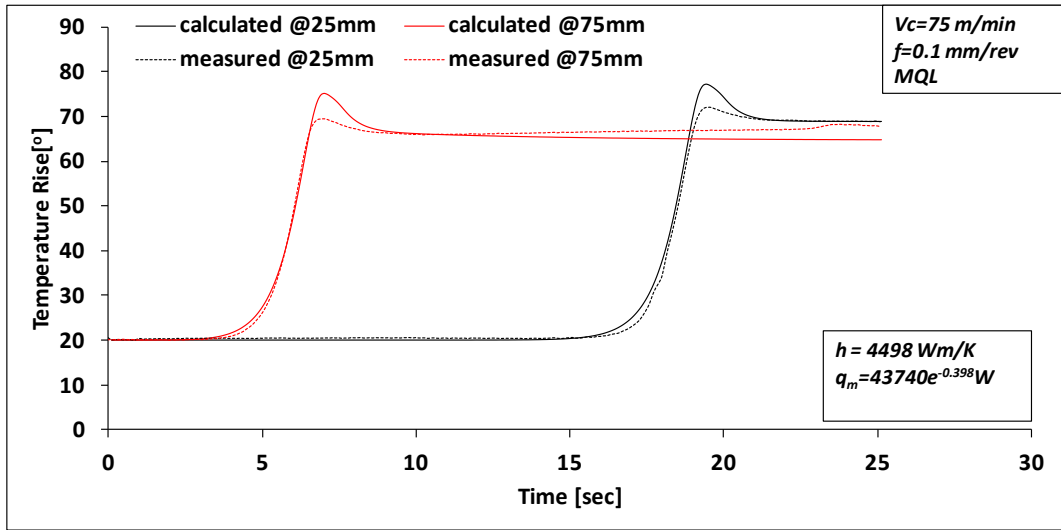


Figure 7. Calculated and measured temperatures during deep-hole drilling.

To model the error between the experimental and modelling data, root mean square error, maximum error and average error are calculated as follows for all thermocouples:

$$RMS = \sqrt{\frac{\sum_1^N (T_{measured} - T_{calculated})^2}{N}} \quad (27)$$

$$e_{max} = \frac{|T_{calculated} - T_{measured}|_{max}}{T_{calculated}} \quad (28)$$

$$e_{ave} = \sum_1^N \frac{|T_{calculated} - T_{measured}|}{T_{calculated}} / N \quad (29)$$

Root mean square error, maximum error and average error for two thermocouples are summarized in Table 3. The temperatures validated by capturing temperatures 1.5 mm away from the machine surface are on two different columns. The maximum errors show the differences among the maximum temperatures, which vary between 5 % and 10 % and the average error varies from 2 % to 3 % for all cutting parameters. Additionally, the root mean square error is also used to judge the accuracy of verification. It shows that the maximum RMS error is 3.2 °C and the average RMS error is 1.5 °C.

Table 3: Root mean square, maximum, average errors, and R-square values

Cutting Parameters	TC1	TC2
$V_c=50 \text{ m/min}$	RMS Error [°C]	2.42
$f=0.15 \text{ mm/rev}$	Maxs. % Error	5%
	Ave. % Error	3%
$V_c=100 \text{ m/min}$	RMS Error [°C]	1.03
		1.40

f=0.15 mm/rev	Maxs. % Error	10%	9%
	Ave. % Error	2%	2%
V_c=100 m/min	RMS Error [°C]	3.20	1.95
f=0.3 mm/rev	Maxs. % Error	8%	7%
	Ave. % Error	2%	2%

Temperature distributions (50^{th} , 150^{th} and, 251^{st} time steps) for all three experiments are presented in Fig. 8. The variation of both heat flux and machining time directly affect temperature distribution. The maximum temperature is observed at the chisel region for all cutting parameters. In simulation of Exp. I ($V_c=25 \text{ m/min}$ $f=0.15 \text{ mm/rev}$), the temperature distributions were more homogenous than any other simulation result due to heat dissipated to the whole body because of longer machining time. Additionally, due to the heat transfer relative to longer machining time, the top surface temperatures were estimated to be equal for all simulations at the last time step (251^{st}), even though heat flux values were different.

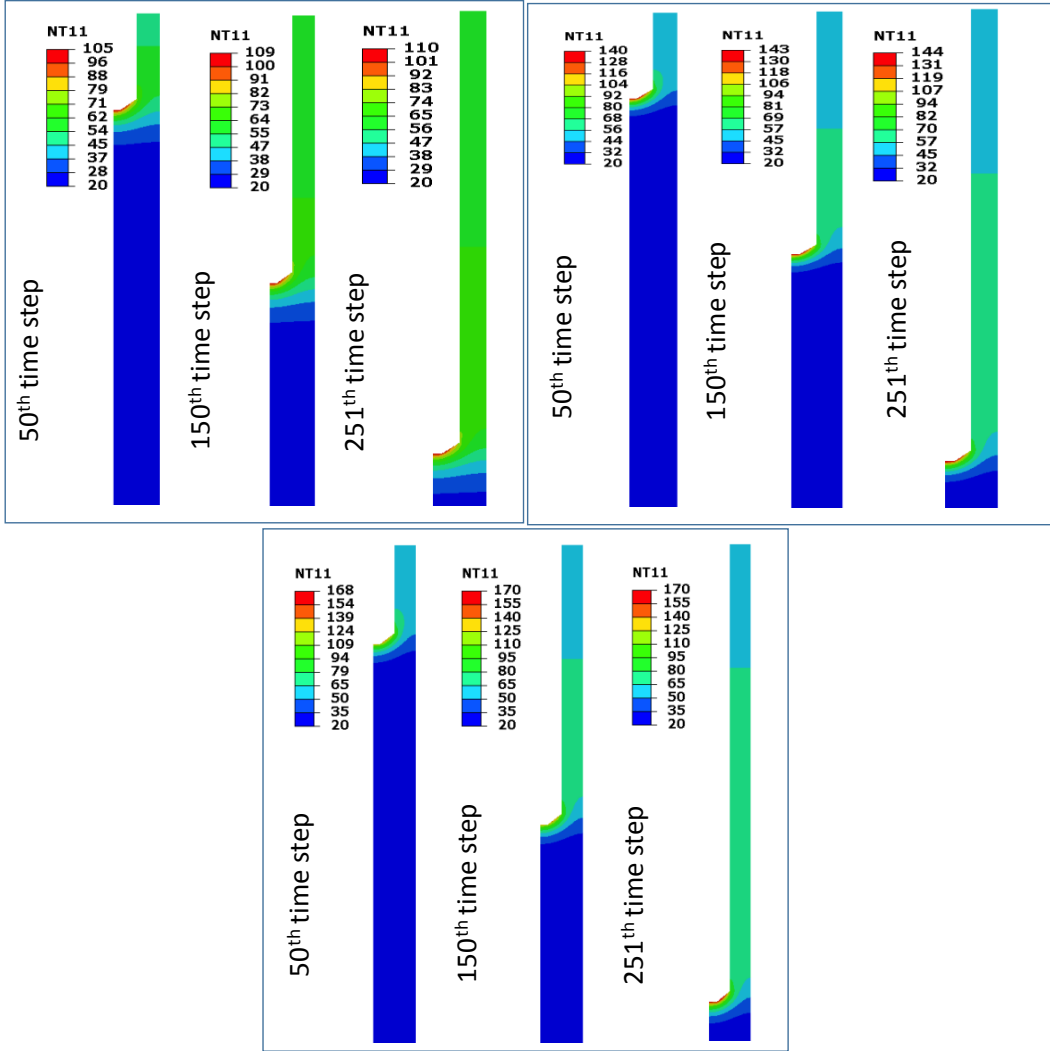


Figure 8. Temperature distributions for cutting parameters of a) Exp. I ($V_c=25$ m/min $f=0.15$ mm/rev) b) Exp. II ($V_c=50$ m/min $f=0.15$ mm/rev) c) Exp. III ($V_c=75$ m/min $f=0.1$ mm/rev) at 50th, 150th and, 251st time steps

Fig. 9a, 9b, and 9c show the temperature distributions between the top surface to 120 mm deep (axial position) and the hole wall to the work piece surface (radial position). Top surface and the center of work piece are defined as zero. In general, three temperature maps are very similar according to their forms. There are two heating effects during deep-hole drilling: The major heating from cutting on the cutting edge and the secondary heating due to the hot chip and friction on the margin, as shown in the graphs. In order to explain the secondary heating effect clearly, the temperatures at the last step on the hole wall (radial position is 5) from the top surface to 120 mm deep are given in Fig. 9d. Although secondary

heating effect of Exp. I and Exp. II were very similar, the highest temperature was observed in Exp. III because of higher heat flux.

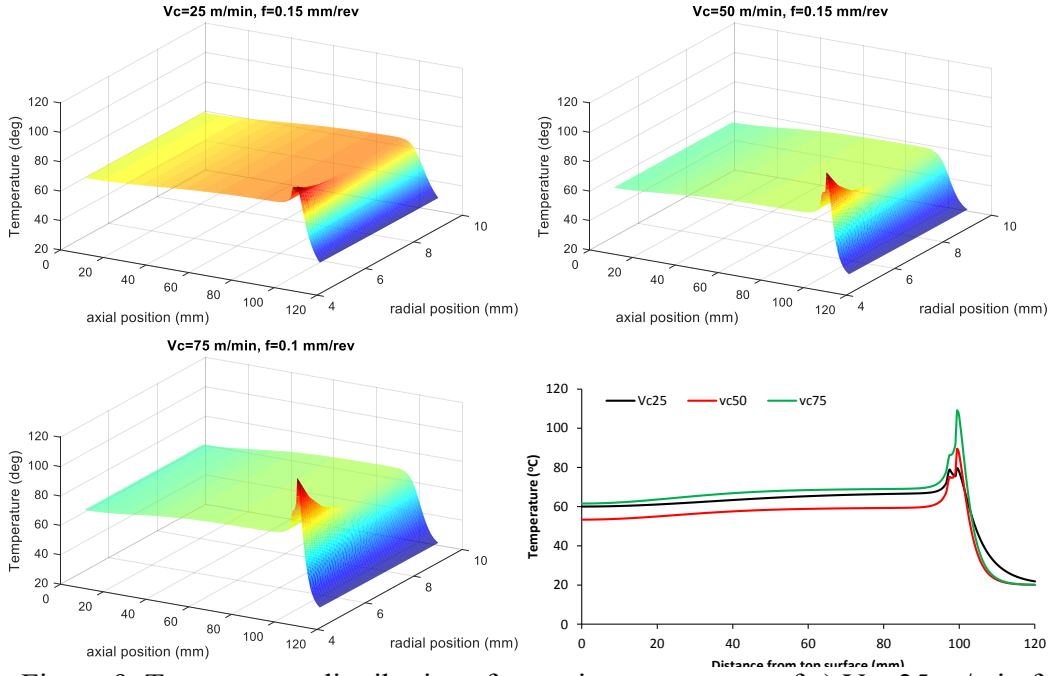


Figure 9. Temperature distributions for cutting parameters of a) $V_c=25$ m/min $f=0.15$ mm/rev b) $V_c=50$ m/min $f=0.15$ mm/rev c) $V_c=75$ m/min $f=0.1$ mm/rev d) on the hole wall (radial position is 5) from top surface to 120 mm deep at last time step

7. CONCLUSION

This paper developed a hybrid thermal model to predict work piece temperature during deep-hole drilling of CGI under MQL cutting condition. The method shows that the temperature distribution strictly depends on the drilling parameters. The main characteristics of the model obtained are as follows;

- A mechanistic approach was used to model thrust force and torque values required to apply the advection heat partition method.
- Heat partition ratios and heat loads along the chisel edge and the cutting lip were estimated using force results that are obtained from the mechanistic model. Heat loads at the margin, generated by hot chips and friction between the drill and hole wall, and the cooling effect of MQL were estimated by the inverse heat transfer method.

- This study significantly contributes to the chip removal procedure by providing a more realistic interpretation of temperatures during drilling. While the drill penetrates into the work piece, the elements were removed sequentially and the heat flux was applied on the subsequent elements in order to model chip removal.
- The thermal model was validated by a direct thermocouple measurement at two different control points. Predicted and experimental results of cutting force and temperatures at the control points were in agreement. Work piece temperature distributions were obtained for different cutting parameters.

Heat distribution on the work piece was calculated for chip removal, the heat load variation along the cutting lip, the chisel and the margin, and the heat convection of oil-air mixture. Through the analysis of the obtained results, the maximum heat flux is identified at the chisel edge, which represents a decreasing trend along the cutting lip from the chisel to periphery of the drill bit. Despite the fact that thrust force and torque values were equal, the heat energy is twice as high when the cutting speed is increased from 25 to 50 m/min under the same feed values.

REFERENCES

- [1] E. Abele, A. Ellermeier, J. Hohenstein, and M. Tschannerl, “Tool length influence on wear behaviour of twisted carbide drills,” *Prod. Eng.*, vol. 1, no. 1, pp. 51–56, 2007.
- [2] B. L. Tai, D. a. Stephenson, R. J. Furness, and A. J. Shih, “Minimum quantity lubrication (MQL) in automotive powertrain machining,” *Procedia CIRP*, vol. 14, pp. 523–528, 2014.
- [3] A. T. Kuzu, A. Bijanzad, and M. Bakkal, “Experimental investigations of machinability in the turning of compacted graphite iron using minimum-quantity lubrication,” *Mach. Sci. Technol.*, vol. 00, pp. 0–18, 2015.

- [4] S. Dawson and T. Schroeder, "Practical Applications for Compacted Graphite Iron," vol. C, no. 05, pp. 1–10, 2004.
- [5] W. M. Mohammed, E. Ng, and M. a. Elbestawi, "Modeling the effect of the microstructure of compacted graphite iron on chip formation," Int. J. Mach. Tools Manuf., vol. 51, no. 10–11, pp. 753–765, 2011.
- [6] F. Mocellin, E. Melleras, W. L. Guesser, and L. Boehs, "Study of the machinability of compacted graphite iron for drilling process," J. Brazilian Soc. Mech. Sci. Eng., vol. 26, no. 1, pp. 18–21, 2004.
- [7] S. Dawson, I. Hollinger, and M. Robbins, "The effect of metallurgical variables on the machinability of compacted graphite iron," Detroit, SAE Tech. Pap., vol. 409, no. 1, pp. 4–16, 2001.
- [8] S. Dawson, "Compacted graphite iron – A material solution for modern diesel engine cylinder blocks and heads performance from smaller engine packages continue to," no. August, pp. 241–246, 2009.
- [9] Watanebe, K., Yokoyuma K., and Ichimaya. R. (1977). "Thermal analyses of the drilling process." Bull. Jpn. Soc. Precis. Eng. 11(2): 71-77. doi:10.2493/jjspe1933.41.1078
- [10] Bono, M. and Ni J. (2001). "The effects of thermal distortions on the diameter and cylindricity of dry drilled holes." International Journal of Machine Tools and Manufacture 41(15): 2261-2270. doi:10.1016/S0890-6955(01)00047-5
- [11] Kalidas, S., Kapoor S. G., and Richard E. DeVor. (2002). "Influence of thermal effects on hole quality in dry drilling, Part 1: A thermal model of workpiece temperatures." Journal of Manufacturing Science and Engineering 124(2): 258-266. doi:10.1115/1.1455645
- [12] Tai, B. L., Stephenson, D. A., and Shih, A. J. (2012). "An Inverse Heat Transfer Method for Determining Workpiece Temperature in Minimum Quantity Lubrication Deep Hole

Drilling." Journal of Manufacturing Science and Engineering 134(2): 021006.

doi:10.1115/1.4005794

[13] Biermann, D., et al. "Thermal aspects in deep hole drilling of aluminium cast alloy using twist drills and MQL." *Procedia CIRP* 3 (2012): 245-250.

[14] Biermann, Dirk, et al. "Simulation of MQL Deep Hole Drilling for Predicting Thermally Induced Workpiece Deformations." *Procedia CIRP* 31 (2015): 148-153.

[15] Segurajauregui, Unai, and Pedro José Arrazola. "Heat-flow determination through inverse identification in drilling of aluminium workpieces with MQL." *Production Engineering* 9.4 (2015): 517-526.

[16] Kuzu, A. T., K. R. Berenji, and M. Bakkal. "Thermal and force modeling of CGI drilling." *The International Journal of Advanced Manufacturing Technology*(2015): 1-14.